



REPORT



Brain pharmacokinetics of anti-transferrin receptor antibody affinity variants in rats determined using microdialysis

Hsueh-Yuan Chang ^a, Shengjia Wu^a, Yingyi Li^a, Wanying Zhang^a, Matthew Burrell^b, Carl I. Webster^b, and Dhaval K. Shah ^a

^aDepartment of Pharmaceutical Sciences, School of Pharmacy and Pharmaceutical Sciences, The State University of New York at Buffalo, Buffalo, NY, USA; ^bAntibody Discovery and Protein Engineering, R&D, AstraZeneca, Cambridge, UK

ABSTRACT

Receptor-mediated transcytosis (RMT) is used to enhance the delivery of monoclonal antibodies (mAb) into the central nervous system (CNS). While the binding to endogenous receptors on the brain capillary endothelial cells (BCECs) may facilitate the uptake of mAbs in the brain, a strong affinity for the receptor may hinder the efficiency of transcytosis. To quantitatively investigate the effect of binding affinity on the pharmacokinetics (PK) of anti-transferrin receptor (TfR) mAbs in different regions of the rat brain, we conducted a microdialysis study to directly measure the concentration of free mAbs at different sites of interest. Our results confirmed that bivalent anti-TfR mAb with an optimal dissociation constant (K_D) value (76 nM) among four affinity variants can have up to 10-fold higher transcytosed free mAb exposure in the brain interstitial fluid (bISF) compared to lower and higher affinity mAbs (5 and 174 nM). This bell-shaped relationship between K_D values and the increased brain exposure of mAbs was also visible when using whole-brain PK data. However, we found that mAb concentrations in postvascular brain supernatant (obtained after capillary depletion) were almost always higher than the concentrations measured in bISF using microdialysis. We also observed that the increase in mAb area under the concentration curve in CSF compartments was less significant, which highlights the challenge in using CSF measurement as a surrogate for estimating the efficiency of RMT delivery. Our results also suggest that the determination of mAb concentrations in the brain using microdialysis may be necessary to accurately measure the PK of CNS-targeted antibodies at the site-of-actions in the brain.

ARTICLE HISTORY

Received 2 November 2020
Revised 28 December 2020
Accepted 6 January 2021

KEYWORDS

Monoclonal Antibody (mAb); brain Pharmacokinetics; large Pore Microdialysis; transferrin Receptor; receptor-Mediated Transcytosis (RMT); brain Capillary Depletion



Introduction


The blood–brain barrier (BBB), which is composed of brain capillary endothelial cells (BCECs) sealed with tight-junctions, greatly restricts the transport of large and hydrophilic molecules from the blood into the brain parenchyma.¹ It has been reported that only 0.1–1% of systemically administered monoclonal antibodies (mAbs) could be distributed into the central nervous system (CNS).^{2–6} Due to this low exposure level, antibody-based therapeutics developed for CNS disorders hardly reach the required therapeutic concentrations at the site-of-action. To enhance the brain distribution of mAbs, many delivery strategies have been developed. Receptor-mediated transcytosis (RMT) is one such established strategy.^{1,7,8} It enhances the brain uptake of mAbs or carrier molecules that bind to endogenous receptors expressed on brain endothelial cells. The receptor-bound mAbs can undergo endocytosis and can be transported to the abluminal side of the brain endothelial cells. The bound mAbs may subsequently dissociate from the receptors and enter the brain parenchyma, where they can perform their pharmacodynamic (PD) effects.^{9–11}

The transferrin receptor (TfR), which is highly enriched in BCECs and choroid plexus epithelial cells (CPECs), is one of the most widely studied for RMT delivery.^{12–14} Much of the existing data have demonstrated the use of TfR-mediated transcytosis to

increase the brain penetration of antibody-based therapeutics (e.g., anti-TfR bispecific mAbs or therapeutic proteins fused with an anti-TfR antigen-binding fragment).¹⁵ However, not all anti-TfR mAbs can reach the brain parenchyma efficiently. A tight binding to TfR may have unintentional side effects of hindering transcytosis and may decrease the fraction of free mAb available in brain parenchyma. Using morphological assessment and the brain capillary depletion method, high-affinity anti-TfR mAbs (e.g., clones OX26, 8D3, and RI7) were found to accumulate within BCECs.^{6,16–18} Conversely, it has been reported that low-affinity variants of anti-TfR mAbs may demonstrate more efficient transcytosis and reach the brain parenchyma at higher concentrations.^{6,19–21}

In addition, the accuracy of using the total anti-TfR mAb concentration in cerebrospinal fluid (CSF) or postvascular supernatant to estimate the free anti-TfR mAb concentration in the brain interstitial fluid (bISF) has yet to be investigated. It has been shown that the distribution of nonspecific mAbs and CNS-targeted mAb is not homogenous and can vary depending on the region of the brain.^{2,22,23} For anti-TfR mAbs, the expression and distribution of endogenous TfRs within CNS may have an impact on their entry into the CNS following systemic administration.

CONTACT Dhaval K. Shah  dshah4@buffalo.edu  Department of Pharmaceutical Sciences, University at Buffalo, the State University of New York, 455 Pharmacy Building, Buffalo, New York 14214-8033.

 Supplemental data for this article can be accessed [here](#).

© 2021 The Author(s). Published with license by Taylor & Francis Group, LLC.

This is an Open Access article distributed under the terms of the Creative Commons Attribution-NonCommercial License (<http://creativecommons.org/licenses/by-nc/4.0/>), which permits unrestricted non-commercial use, distribution, and reproduction in any medium, provided the original work is properly cited.

To better understand the effect of affinity on RMT of anti-TfR mAbs, and to establish quantitative relationships between the exposures of these molecules in different regions of the brain, including the site-of-action, we investigated the disposition of bivalent anti-TfR mAbs with varying affinity in different regions of the rat brain using a push-pull microdialysis system for mAbs.² Although the push-pull microdialysis procedure for mAbs is challenging and requires extensive training,^{2,24} it can provide direct *in vivo* measurement of free anti-TfR mAb concentration in selected regions of the brain in freely moving animals. It can avoid the detection of bound mAbs on the BCECs and the neurons, and such readout of free mAb concentration in the brain interstitial fluid (bISF) tends to better represent the required therapeutic concentration at the site-of-action. Further, simultaneous quantification of the anti-TfR mAb exposure in different regions of the brain using microdialysis may help us better understand the extent of enhanced delivery of anti-TfR mAbs in different regions of the CNS.

Results

Plasma pharmacokinetics of OX26 variants following 10 mg/kg i.v. administration

The plasma pharmacokinetics (PK) of bivalent OX26 variants intravenously (i.v.) administered at a 10 mg/kg dose are shown in Figure 1, and the results from non-compartmental analysis of the PK data are shown in Table 1. The mAbs were found to demonstrate target-mediated drug disposition (TMDD),²⁵ and OX26-5 variant was found to have the fastest plasma clearance and shortest half-life ($t_{1/2}$). Interestingly, when the equilibrium dissociation constant (K_D) value was increased to 174 nM, the OX26-174 variant appeared to lose its *in vivo* binding to TfRs, and its plasma PK was found to be similar to our previously published plasma PK for a nonspecific mAb (i.e., trastuzumab; Supplementary Figure 1).²

CNS PK of OX26 variants measured using microdialysis following 10 mg/kg i.v. administration

The CNS PK of OX26 variants is shown in Figure 2, and the results from non-compartmental analysis of the PK data are shown in Table 1. The high-affinity OX26-5 variant had the lowest area under the concentration curve (AUC) value in CSF and the bISF. When the K_D values were increased from 5 nM to 76 and 108 nM, the bISF AUC and the CSF at the cisterna magna (CSF_{CM}) AUC values significantly increased (Table 1, Figure 2a–d). As such, enhanced brain delivery of free-form OX26 variants at bISF via RMT was observed by an adequate reduction in binding affinity for the target (Figure 2c). The enhanced brain delivery appeared to be more noticeable when the bISF-to-plasma concentration ratios and bISF-to-plasma AUC ratios were computed (Figure 2g, Table 1). Amongst the four different binding affinity variants of bivalent anti-TfR

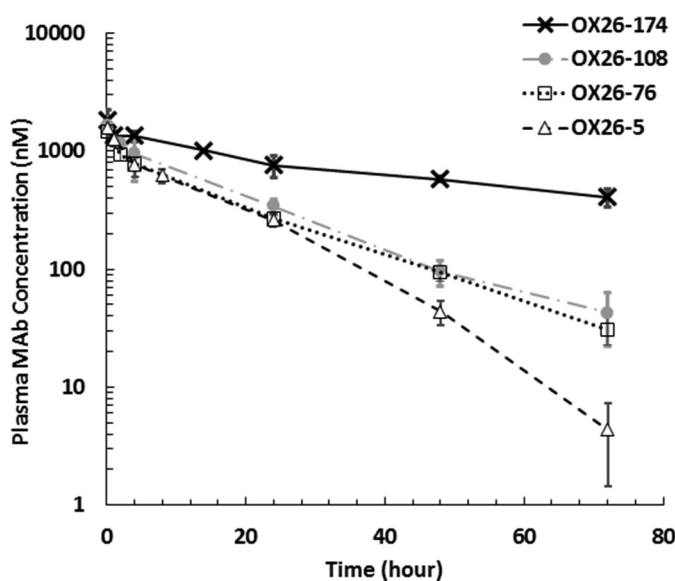


Figure 1. *In vivo* plasma PK profiles of anti-TfR antibody affinity variants following 10 mg/kg systemic administration in rats. Open triangle: OX26-5 ($K_D = 5$ nM), open square: OX26-76 ($K_D = 76$ nM), closed circle: OX26-108 ($K_D = 108$ nM), cross: OX26-174 ($K_D = 174$ nM). Error bar: standard deviation.

Table 1. Non-compartmental analysis of plasma and brain PK profiles of anti-TfR antibody affinity variants in rats.

	unit	OX26-5	OX26-76	OX26-108	OX26-174
Plasma $AUC_{0 \rightarrow t_{last}}$	$nM \cdot h \cdot L^{-1}$	18500 (750)	20400 (640)	21900 (1170)	54300 (1770)
bISF _{ST} $AUC_{0 \rightarrow t_{last}}$	$nM \cdot h \cdot L^{-1}$	69.3 (5.9)	671 (74.6)	450 (135)	151 (20)
CSF _{LV} $AUC_{0 \rightarrow t_{last}}$	$nM \cdot h \cdot L^{-1}$	33 (4.4)	117 (17)	114 (11.4)	154 (23.4)
CSF _{CM} $AUC_{0 \rightarrow t_{last}}$	$nM \cdot h \cdot L^{-1}$	45.4 (12.7)	180 (28.5)	158 (25.5)	160 (16.9)
Brain $AUC_{0 \rightarrow t_{last}}$	$nM \cdot h \cdot L^{-1}$	248 (35)	1540 (140)	613 (23.5)	158 (17.5)
$AUC_{bISF(ST)}/AUC_{Plasma}$	%	0.37	3.29	2.05	0.28
$AUC_{CSF(LV)}/AUC_{Plasma}$	%	0.18	0.58	0.52	0.28
$AUC_{CSF(CM)}/AUC_{Plasma}$	%	0.25	0.89	0.72	0.29
AUC_{Brain}/AUC_{Plasma}	%	1.34	7.5	2.8	0.29
Plasma $t_{1/2}$	h	8.12	15.3	16.7	53.5
bISF _{ST} $t_{1/2}$	h	12.1	16.2	17.4	- ^a
CSF _{LV} $t_{1/2}$	h	20.6	25.0	27.2	- ^a
CSF _{CM} $t_{1/2}$	h	12.1	37.0	20.9	77.8 ^a

AUC: the area under the concentration curve, t_{last} : the last time point (72 h), bISF: brain interstitial fluid, ST: striatum, CSF: cerebrospinal fluid, LV: lateral ventricle, CM: cisterna magna, $t_{1/2}$: half-life; the K_D values for OX26-5, OX26-76, OX26-108, and OX26-174 are 5, 76, 108, and 174 nM, respectively. Standard deviation in parentheses. Note: ^athe observation time was not long enough to accurately estimate the $t_{1/2}$.

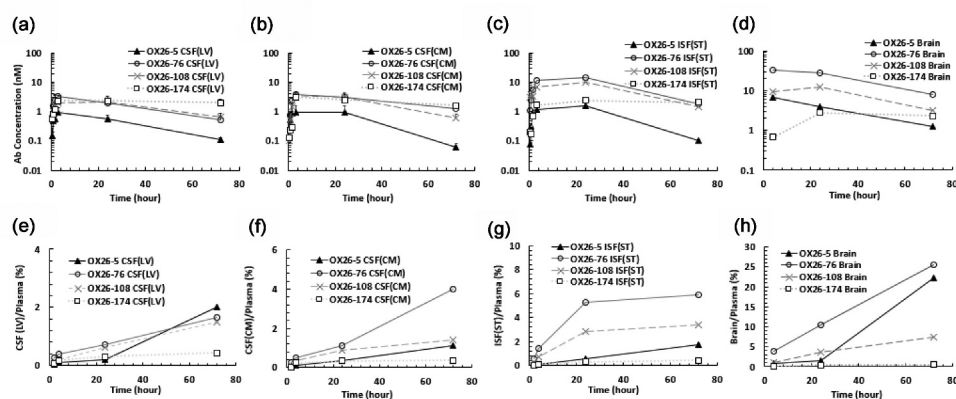


Figure 2. *In vivo* PK of anti-TfR antibody affinity variants in different regions of the rat brain following 10 mg/kg systemic administration. (a)–(c) Free OX26 variant concentrations in: (A) cerebrospinal fluid (CSF) at the lateral ventricle (LV), (b) CSF at the cisterna magna (CM), and (C) brain interstitial fluid (ISF) at the striatum (ST). (d) Total OX26 variant concentrations in the whole brain homogenate. (e)–(g) CNS-to-plasma concentration ratios for unbound OX26 variants over the time. (E) CSF_{LV}-to-plasma, (f) CSF_{CM}-over-plasma, (G) ISF-to-plasma. (h) Brain-to-plasma concentration ratios for total OX26 variants. Closed triangle: OX26-5 ($K_D = 5$ nM), open circle: OX26-76 ($K_D = 76$ nM), mark: OX26-108 ($K_D = 108$ nM), open square: OX26-174 ($K_D = 174$ nM); LV: lateral ventricle, CM: cisterna magna, ST: striatum, error bar: standard deviation.

mAbs evaluated, we found OX26-76 with a moderate affinity ($K_D = 76$ nM) to be the better enhancer of TfR-mediated transcytosis at 10 mg/kg dose, which increased bISF-to-plasma AUC ratio by more than 10-fold compared to OX26-174 and nonspecific mAbs.² A threshold in the binding affinity value for OX26 variants to accomplish TfR-mediated transcytosis in the CNS *in vivo* was also observed. As the K_D value increased to 174 nM, the observed AUC values of OX26-174 in CSF, ISF, and brain were found to be similar to that of previously published nonspecific mAbs (trastuzumab) at the same dose (Supplementary Figures 2 and 3).² A bell-shaped relationship between the K_D values and the AUC values of OX26 variants in bISF and brain homogenate was observed, which is shown in Figure 3a. However, no clear correlation was observed between the CNS exposure and dissociation rate constant (k_{off}) of antibodies (Figure 3b).

It was also observed that the beneficial effect of RMT might vary in different regions of the brain (Figure 2e–h). While OX26-76 with the optimal binding affinity significantly enhanced the mAb delivery into bISF and CSF_{CM}, it did not

significantly increase the CSF at the lateral ventricles (CSF_{LV})-to-plasma concentration ratios. This may suggest that at the lateral ventricles (LV), where the formation of the CSF and potential entry of mAbs into the CSF via nonspecific pathways occurs, the contribution of the TfR-mediated transcytosis pathway may not be as prominent compared to other pathways.²

In vivo PK of OX26 variants in brain homogenate, brain capillaries, and postvascular supernatant following 10 mg/kg i.v. administration

To examine the accumulation of OX26 variants in BCECs, the brain capillary depletion approach was used.²⁶ The PK of all four OX26 variants in plasma, bISF, whole brain, brain capillaries, and postvascular supernatant is shown in Figures 2d,h and 4. OX26-5, OX26-76, and OX26-108 were found to accumulate in isolated brain capillaries. The BCEC concentration of OX26-5 and OX26-76 were found to be even higher than plasma concentrations at 72 hours after administration. The OX26-174 variant was not found to accumulate in BCECs to

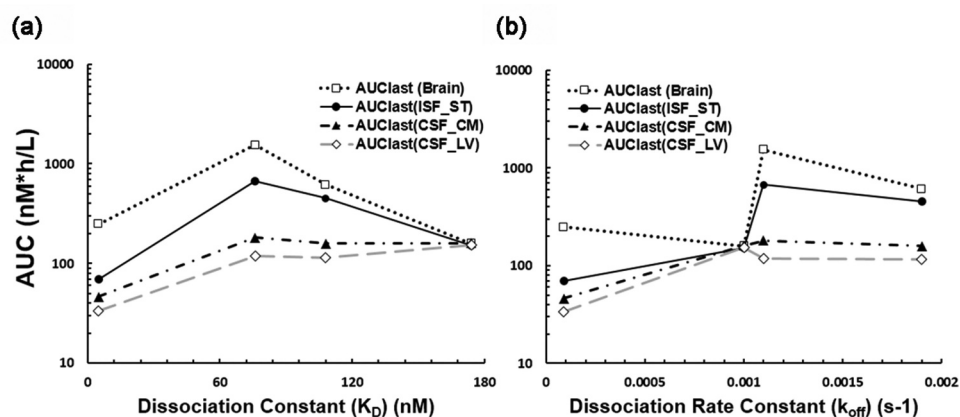


Figure 3. The influence of binding kinetic parameters to antibody exposure in the central nervous system. (a) The relationship between the AUC in different regions of the brain after 10 mg/kg *i.v.* administration of OX26 variants in rats and dissociation constants (K_D) for TfR. A bell-shaped relationship was observed in the ISF and brain, but not in the CSF compartments. (b) The relationship between the AUC and dissociation rate constants (k_{off}). AUC was computed from time 0 to the last time point (72 h). Open square: AUC_{brain}, closed circle: AUC_{ISF(ST)}, closed triangle: AUC_{CSF(CM)}, and open diamond: AUC_{CSF(LV)}. AUC: area under the concentration curve, ISF: interstitial fluid, CSF: cerebrospinal fluid, ST: striatum, CM: cisterna magna, LV: lateral ventricle.

a significant level (Figure 4), which corresponds to reduced TfR binding of this variant.

Discussion

Our study presents the application of intracerebral microdialysis to measure the concentrations of different anti-TfR antibody affinity variants in different regions of the rat brain. Since tissue-bound antibody molecules cannot cross the microdialysis probe membrane, it is commonly assumed that all the molecules measured using microdialysis represent free mAb concentrations.²⁴ Although the setup of microdialysis system can be arduous, it allows an opportunity to directly measure free mAb concentrations in bISF of living animals, without any manipulation of brain samples. Additionally, microdialysate is substantially clean and devoid of complex tissue matrix, which prevents potential contamination of the sample via redistribution of bound anti-TfR mAbs from cell lysates. One of the main challenges for applying the large-pore microdialysis system to measure the concentrations of mAbs is the difficulty in measuring *in vivo* probe recovery. This is mainly due to the limitation of current analytical methods that cannot accurately and precisely measure the low probe recovery of 150 kDa IgG molecules using the retrodialysis approach.^{2,27} Therefore, the *in vitro* probe recovery is used as a surrogate for the *in vivo* probe recovery. Nonetheless, based on previous investigations, it is typically assumed that there is no significant difference in the probe recovery of mAbs when measured via *in vivo* and

in vitro methods.^{2,28} To avoid any error in the measurement of mAb concentrations due to the catabolites, which is typically observed with imaging and radiolabeling methods,²⁹ here we used sensitive and specific sandwich enzyme-linked immunosorbent assay (ELISA) methods to quantify full-length IgGs in all samples.

In attempting to exploit TfRs to accomplish transcytosis of mAbs in the brain, it has been recognized that the binding affinity of mAb toward TfRs is one of the critical parameters that determines the intracellular trafficking behavior of the antibody (along with the avidity).¹³⁻¹⁵ The observed bell-shaped relationship between the K_D value of bivalent anti-TfR mAbs and the exposure of free anti-TfR mAbs in bISF is consistent with the previously reported work in rodent brain homogenates.^{6,19-21,30,31} It should also be emphasized that anti-TfR bivalent mAbs used in this study were engineered to bind to the same epitope on TfRs. This feature may help us more directly examine the effect of the binding affinity on the brain uptake of anti-TfR mAbs.^{20,21,31} The optimal affinity of bivalent anti-TfR mAbs for higher efficiency in TfR-mediated transcytosis in the mouse brain has been found to be 111 nM (IC_{50}) at a 20 mg/kg dose.⁶ However, this optimal binding affinity could be dose-dependent, and may be shifted to a higher IC_{50} value (~588 nM) at a higher dose (50 mg/kg).^{19,30} Monovalent anti-human TfR mAbs have been reported to demonstrate similar optimal affinity range ($K_D = \sim 270$ nM) to accomplish transcytosis in the brains of human TfR transgenic mice at a 50 mg/kg dose.³² In this study, the optimal

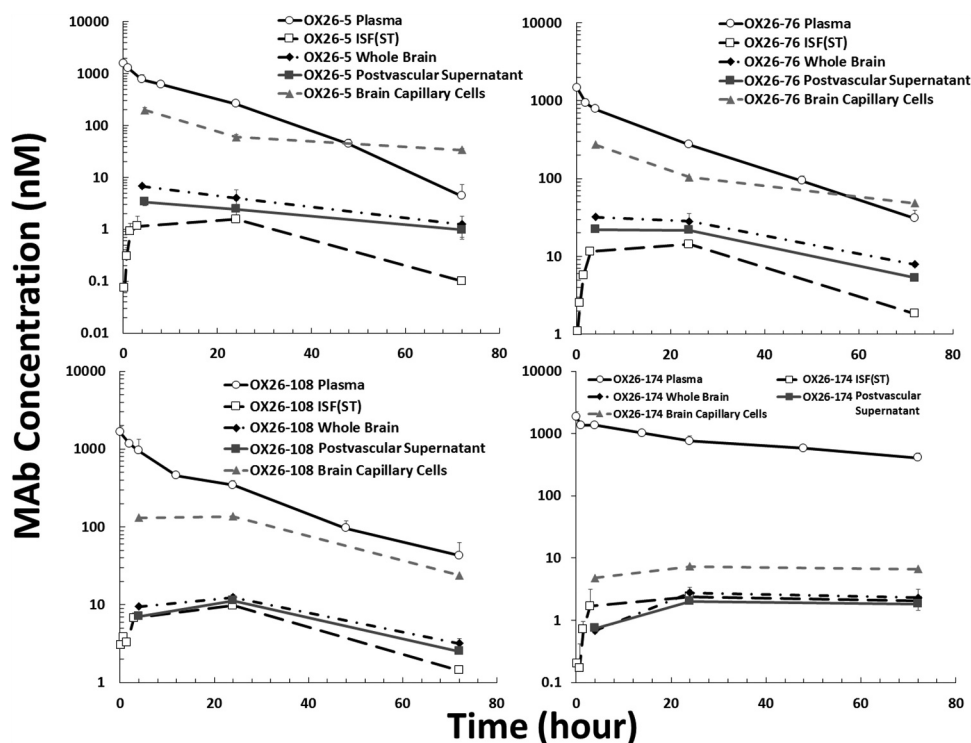


Figure 4. *In vivo* PK of anti-TfR antibody affinity variants (OX26-5, OX26-76, OX26-108, and OX26-174) in rat plasma, brain interstitial fluid, whole-brain homogenate, isolated brain capillaries, and postvascular supernatant. The animals received 10 mg/kg i.v. dose of antibodies via the tail vein. Upper left: OX26-5 ($K_D = 5$ nM), upper right: OX26-76 ($K_D = 76$ nM), bottom left: OX26-108 ($K_D = 108$ nM), bottom right: OX26-174 ($K_D = 174$ nM). Open circle: plasma, open square: brain ISF, closed diamond: whole brain, closed square: postvascular supernatant, and closed triangle: isolated brain capillaries. The error bar presents the standard deviation.

affinity of bivalent anti-TfR mAbs to accomplish TfR-mediated transcytosis in the rat brain at a 10 mg/kg dose was found to be 76 nM, amongst the four different variants evaluated ($K_D = 5, 76, 108, \text{ and } 176$). This optimal K_D value was found to be slightly higher (76–108 nM) in our previous study at 20 mg/kg dose in rats.²¹ The optimal affinity has been reported to shift to a lower K_D value of ~37 nM in nonhuman primates at a dose of 30 mg/kg.³² These observations suggest that the functionality and the nature of the endogenous TfR (e.g., location, expression, intracellular trafficking) may vary across different species. Therefore, to translate the preclinical data for TfR-mediated transcytosis of mAbs to the clinical, the difference in the intrinsic behavior of TfRs and the brain physiology between different species, as well as how the molecular format of an antibody affects intracellular trafficking of the transcytosis receptor across different species, should also be considered.

The potential mechanisms for less efficient RMT of high-affinity anti-TfR mAbs have been discussed widely.^{13–15} This phenomenon could be explained by different models, which may happen simultaneously. First, a high-affinity binding may reduce the chance of mAbs to dissociate from TfRs at the BCECs, resulting in entrapment of the mAb with TfRs toward the lysosomal degradation process (regardless of the avidity).^{6,19} Conversely, a low-affinity anti-TfR mAb can dissociate from TfRs at the abluminal side or at the acidic pH of the late endosome,^{6,33} resulting in the successful delivery of the mAb at the abluminal side. Second, high-affinity bivalent anti-TfR mAbs may have a higher likelihood to cause dimerization of TfR and can alter the intracellular trafficking toward lysosomal degradation. In fact, more than 50% reduction in the TfR expression has been found following the administration of high-affinity bivalent anti-TfR mAbs.¹⁹ This intracellular sorting of high-affinity anti-TfR mAbs to late endosomes has been reported in mice and rats.^{19,20} This higher lysosomal degradation caused by a high binding affinity may explain our observation where we saw lower intact OX26-5 concentrations in the isolated brain capillaries at 24 and 72 hours after administration compared to OX26-76. This timeframe is consistent with the initiation of TfR downregulation reported in previous *in vitro* studies (48 hours for bivalent anti-TfR mAbs at 1.25 μM concentration,²⁰ and 24 hours for bivalent anti-TfR mAbs at 2.5 $\mu\text{g/mL}$ concentrations).¹⁵ However, Bien-Ly et al. have reported a longer time for *in vivo* downregulation of TfR following administration of high-affinity monovalent anti-TfR mAbs in mice,¹⁹ where they did not find a significant reduction of TfR at 24 hours but observed the reduction at the next time point (i.e., 96 hours). This difference in lysosomal degradation could be species-dependent or valency-dependent.

Here we also report that the extent of enhanced CNS delivery via RMT may vary depending on the region of the brain (Figure 3). The most optimal anti-TfR antibody affinity variant OX26-76 was found to increase bISF-to-plasma AUC ratio by more than 10-fold when compared to OX26-174. Although TfR is expressed on both the BCECs and the CPECs, the CSF_{LV}-to-plasma AUC ratio was only 2-fold higher for OX26-76 when compared to OX26-174. In fact, the difference in CSF_{LV}-to-plasma concentration ratios for the four OX26

variants was found to be insignificant (Figure 2e). This may suggest that the contribution of TfR-mediated transcytosis toward the entry of OX26 variants into CSF_{LV} could be less significant compared to other nonspecific pathways operating at the blood-CSF barrier (BCSFB). In fact, our previous study suggested that the entry of nonspecific mAbs into the LV via BCSFB would be one of the earliest pathways for mAb entry into the CSF following systemic administration.²

On the other hand, we observed that the exposure of the OX26 variant with an optimal binding affinity to TfR increased more significantly at the CSF_{CM} (Figure 2f and Table 1). Considering high concentrations of transcytosed OX26-76 in the bISF, this enhanced exposure of OX26-76 at CSF_{CM} could be due to the influx of transcytosed mAb from the brain parenchyma into the CSF_{CM} potentially via a perivascular pathway.^{34,35}

We also observed that the identification of optimal K_D value for enhanced free mAb exposure at the bISF could also be accomplished using whole-brain homogenate concentrations (Figure 3), despite the potential accumulation of OX26 variants within the BCECs. This may be due to the fact that the transcytosed amount of mAbs in brain parenchyma can overwhelm the amount of mAbs trapped onto a limited number of TfRs.

To examine the accumulation of OX26 variants in BCECs, we isolated the BCECs from the brain for analysis. Interestingly, we observed that OX26-76 had significantly higher BCEC concentrations than OX26-5 at 24 and 72 hours after administration (p -value <0.05 and <0.01 , respectively). Since we quantified only the full-length IgG and excluded the catabolized fragments from quantification, the lower accumulated concentrations of OX26-5 in the isolated capillary may suggest the presence of higher lysosomal degradation for this high-affinity anti-TfR mAb.^{15,19,20} We also observed that it is challenging to use the brain capillary-depletion method as a surrogate to accurately estimate the free OX26 concentrations in bISF. OX26 variant concentrations in bISF measured using microdialysis in our study were found to be almost always lower than the soluble mAb concentrations measured in postvascular supernatant. This discrepancy stems from the redistribution of a fraction of mAb bound to the intraneuronal endogenous TfR to postvascular supernatant during the sample preparation.^{12,36–38} Interestingly, we found that the total concentrations of OX26-76 in postvascular supernatant were two-fold higher than OX26-108 concentrations at 24 and 72 hours after administration (p -values <0.05). This difference between OX26-76 and OX26-108 was not present when their “free” AUC values in bISF were compared (Table 1). This observation suggests that the lower K_D value of OX26-76 may result in higher binding of this mAb to TfRs expressed in brain parenchyma compared to OX26-108.

In summary, here we demonstrated the application of a large-pore microdialysis system to directly measure the concentrations of transcytosed free anti-TfR antibody affinity variants in different regions of the brain. We confirm a bell-shaped relationship between the K_D value and antibody exposure in the bISF for anti-TfR mAbs using our orthogonal experimental method. We found that the contribution of TfR-mediated transcytosis for enhancing mAb delivery in the brain was less

significant at the BCSFB compared to the BBB. This observation highlights the challenge in using CSF measurement as a surrogate for antibody exposure at the site-of-action and estimating the efficiency of RMT delivery. We also observed that, despite the discrepancy between total mAb exposure in brain homogenate and free mAb exposure in bISF, both the measurements were able to identify the same optimal binding affinity value for maximum RMT of anti-TfR mAbs. In addition, we observed that mAb concentrations measured in post-vascular supernatant after capillary depletion were almost always higher than the mAb concentrations in bISF measured using microdialysis. This suggests that microdialysis may be necessary to accurately measure the PK of CNS-targeted antibodies at the site-of-action in the brain.

Materials and methods

Antibody preparation and characterization

Production and characterization of chimeric mouse-human anti-rat TfR antibody OX26 and its affinity variants was performed as described previously.²¹ The affinity of all antibodies was determined using the Octet RED384 System (Pall ForteBio LLC, Fremont, CA,) with Anti-hIgG Capture Biosensors (18--5060, Pall ForteBio LLC) and TfR extracellular domain in solution. The K_D values for OX26-5, OX26-76, OX26-108, and OX26-174 mAbs were 5 ± 2 , 76 ± 10 , 108 ± 30 , and 174 ± 43 nM, respectively.²¹ For all studies, the antibodies were expressed in Chinese hamster ovary cells and purified using protein-A column followed by size exclusion chromatography, as previously described.^{20,21}

Animals and surgery

The animal protocol was approved by Institutional Animal Care and Use Committee of University at Buffalo. The procedure of microdialysis surgery was as previously described.² Briefly, 6-week-old male Sprague Dawley rats (Taconic Biosciences, USA) weighing 170–220 g were anesthetized and placed in a dual-arm stereotaxic frame (Cat. # 51503, Stoelting Co., USA) at a flat head position (i.e., the bregma and the lambda are in the same horizontal plane). The animals were instrumented with two AtmosLM guide cannulas (PEG-x, Eicom, USA) in the following three different combinations of the striatum (ST), the LV, and the cisterna magna (CM): ST+LV, ST+CM, or LV+CM. These regions would present the free mAb concentration in CSF at the formation site (LV), the downstream of the CSF circulation (CM), and the bISF (ST), the expected site-of-action for many CNS-targeted mAbs.

For the ST, the coordinate of the microdialysis guide was: 1.0 mm anterior, 3.0 mm lateral, and 6.0 mm ventral relative to bregma. For the LV, the coordinate of the microdialysis guide was: 1.1 mm posterior, 1.8 mm lateral, and 5.4 mm ventral relative to the bregma. For the CM, the coordinate of the microdialysis guide was: 2.51 mm posterior, 2.04 mm lateral, and 9.0 mm ventral, at an angle of 25° from the dorsoventral axis (toward anterior) and 11° lateral from the anteroposterior

axis relative to lambda. The coordinate was validated by checking the brain tissue section after local injection of methyl-blue dye via the microdialysis guide cannula. The validation details have been discussed in our previous study.²

The ST and LV were instrumented with guide cannulas (PEG-8, Eicom, USA) and dummy probes (PED-8, Eicom, USA) whose shaft length is 8 mm, whereas the CM was instrumented with a longer guide cannula (PEG-12, Eicom, USA) and a dummy probe (PED-12, Eicom, USA) that has a 12 mm long shaft. Four anchor screws (Cat. # CMA7431021, Harvard Apparatus, USA) were mounted on the surface of the skull with dental cement and glass ionomer cement for permanent head attachment (Cat. # MGIG/AKIT2, Instech Laboratories, USA). After the surgery, 5 mg/kg carprofen (Rimadyl®) was given subcutaneously once per day for 48 h, and the animals were allowed to recover for 10 days before *in vivo* microdialysis experiments. One night prior to the experiment, the dummy probes were replaced with the AtmosLM microdialysis probes (PEP-x-1, 1000 kDa MWCO, membrane material: polyethylene 0.44 mm OD, shaft: 0.58 mm OD/0.5 mm ID, Eicom, USA).

Experimental setup for push-pull microdialysis

The experimental setup has been previously described.² Briefly, as shown in Figure 5, a CMA 402 syringe pump (Cat. # CMA8003100, Harvard Apparatus, USA) and 2.5 mL microsyringes (Cat. # CMA8309021 Harvard Apparatus, USA) were used to perfuse the artificial CSF (aCSF) (150 mM sodium, 3 mM potassium, 1.4 mM calcium, 0.8 mM magnesium, 155 mM chloride, and 0.15% bovine serum albumin) as a push pump system. Fluorinated ethylene propylene (FEP) tubing (Cat. # BFEP-T22Q, Instech Laboratories, USA) was used to connect the syringe pump to the AtmosLM microdialysis probe and subsequently to the Harvard peristaltic pump P-70 (Cat. # 70–7000, Harvard Apparatus, USA). The peristaltic pump was equipped with 3-Stop PVC tubing (Cat. # 72–0654, Harvard Apparatus, USA) and pulled microdialysate from the probe to the sampling tube (Cat. # L250902, Laboratory Products Sales, USA). The connections of FEP tubing were secured by 0.015-inch silicone tubing connectors (Cat. # MC015/10, Instech Laboratories, USA).

Before the experiment, the syringe pump was calibrated, and the flow rate was set to 1 μ L/min. Then, the flow rate of the peristaltic pump was calibrated to 1–1.03 μ L/min by measuring the output of the microdialysate. The probe was conditioned with 70% ethanol and perfused with aCSF to remove the air bubbles. Then it was connected to the push-pull pumps. After microdialysis, the *in vitro* probe recovery of antibodies was determined using a standard solution of 1000 ng/mL OX26 variants prepared in aCSF. The *in vitro* recovery for each microdialysis probe was defined as the ratio of the concentration in the dialysate ($C_{\text{dialysate}}$) over the reservoir concentration ($C_{\text{reservoir}}$).^{2,24} The *in vitro* probe recovery (1 mm membrane) for OX26 variants was ~3%.

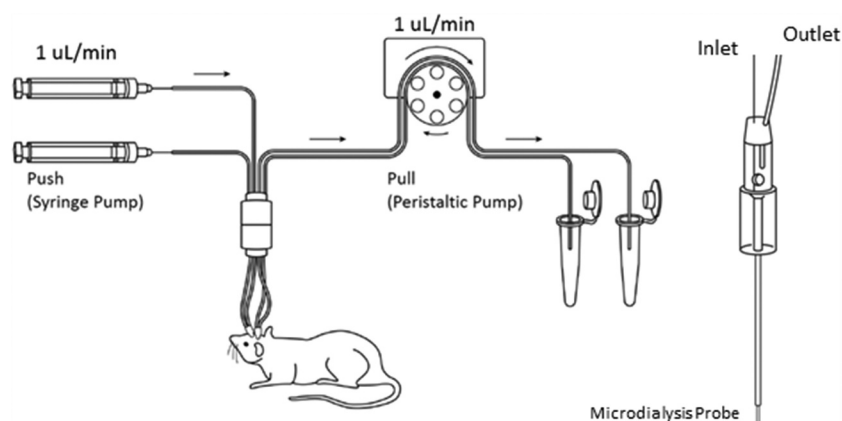


Figure 5. The Push-Pull system for large-pore microdialysis. The system requires both a syringe pump and a peristaltic pump to maintain a consistent flow rate before and after the microdialysis probe. The microdialysis probe has an open vent to keep the inner fluid pressure constant and prevents ultrafiltration of perfusion fluid from the probe into the brain tissue. More details have been discussed in Ref 2.

In vivo plasma and CNS PK study of OX26 variants in rats

The details of the procedure have been discussed in our previous study.² Briefly, after 10-day recovery from the surgery, rats were anesthetized with isoflurane and dosed (i.v.) with 10 mg/kg of anti-TfR mAbs via tail vein injection. Blood samples were collected via the lateral saphenous vein in EDTA-precoated tubes and were centrifuged at 4000 rcf for 10 minutes at 4°C. Plasma was then collected and stored at -20°C for further analysis. Brain microdialysates of bISF_{ST}, CSF_{LV}, and CSF_{CM} were collected using microdialysis (0–30, 30–60 min, 1–2, 2–4, 22–24, and 74–76 h after i.v. administration). Each fraction of microdialysate was collected in a 1.5 mL siliconized microcentrifuge tube (Cat. #L250902, Laboratory Products Sales, USA) and was stored at -20°C until analysis. After microdialysis, rats were anesthetized, and terminal blood samples were collected using cardiac puncture. Immediately after terminal blood sampling, the whole body was perfused with 30 mL cold phosphate-buffered saline (PBS) buffer. Half of the brain was further perfused via the carotid artery with 2.5 mL cold 1X PBS. After perfusion, the perfused half of the brain was transferred to a 15 mL tube and frozen in liquid nitrogen. Then, the brain tissue was weighed and stored at -80°C until brain capillary depletion and further analysis.

Brain capillary depletion and homogenization

The brain capillaries were isolated from the brain using the brain capillary depletion method.²⁶ Briefly, the brain was weighed and diluted 1:1 with physiologic buffer (pH 7.4, 10 mM HEPES, 141 mM NaCl, 4 mM KCl, 2.8 mM CaCl₂, 1 mM MgSO₄, 1 mM NaH₂P0₄, and 10 mM D-glucose), followed by homogenization. The suspension was mixed at 1:1 ratio with 26% dextran solution (final concentration of dextran is 13%). After taking an aliquot of the brain homogenate, the remainder was centrifuged at 5,400 g for 15 min at 4°C. The supernatant and pellet were carefully separated. The pellet was assumed to

consist of brain vasculature according to the previously published protocol.²⁶ The intactness of isolated cells was confirmed using a microscope, and the supernatant was considered to be devoid of the vasculature. The whole brain, postvascular supernatant, and the brain capillaries were weighed and further homogenized with RIPA buffer (Cat. # 89900, Thermo Fisher Scientific, USA) containing 1X Halt™ protease inhibitor (Cat. # 78430, Thermo Fisher Scientific, USA) using BeadBug microtube homogenizer (Cat. # D1030, Benchmark, 3.0 mm beads, USA). The homogenate was further diluted with the RIPA buffer and incubated on ice with gentle shaking for 2 h. After incubation, the brain homogenate was centrifuged (15 mins, 4°C, 15000 rcf) to remove cell debris.

Brain cryostat sectioning to validate the placement of the inserted microdialysis probes

After the microdialysis experiment and terminal blood sampling, 2 µL of methylene blue was perfused into the brain compartments via the microdialysis guide cannula as we previously described.² Brain tissue was collected and placed in a small boat containing tissue freezing medium (Cat.# TFM-5, General Data, USA). The small boat was gradually frozen using liquid nitrogen until the medium was completely hardened. The cube was stored at -80°C overnight. Before the cryostat section, the frozen brain in the hardened freezing medium was transferred to a -20°C freezer and kept for 1 h. Brain tissue was then sectioned using Microm HM 525 (Cat.# 956640, Thermo Fisher Scientific, Microm International GmbH, Germany).

Quantification of chimeric mouse-human OX26 variants and trastuzumab in plasma, microdialysate, and brain homogenate using ELISA

The ELISA protocols for quantification of full-length anti-TfR OX26 variants (chimeric mouse-human IgG) and

trastuzumab (humanized IgG) in rat matrices have been developed as previously described.² The format of the sandwich ELISA was kept the same. The preparation of the standard solution varies for different matrices. Goat anti-human IgG-Fc fragment cross-adsorbed antibodies (Cat. # A80-304A, Bethyl Laboratories, USA) were diluted to 5 µg/mL in 20 mM Na₂HPO₄ buffer. The Nunc[®] Maxicorp™ 384-well plate (Cat. # 142761, Thermo Fisher, USA) was then coated with 35 µL/well diluted anti-human IgG-Fc antibodies and incubated at 4°C overnight. The plate was washed three times with PBS-Tween (0.05% Tween-20 in 1X PBS), followed by three times of wash with distilled water using the AquaMax2000 plate washer (Cat. # AQUAMAX 2 K, Molecular Devices, Sunnyvale, CA). The plates were then blocked with 90 µL/well of ELISA blocking solution (Cat. # E104, Bethyl Laboratories, USA) and incubated at room temperature (RT) for 1 h on a plate shaker. After the incubation, the plate was rewashed and loaded with 30 µL/well of samples and the standards of chimeric OX26 variants. All the standards were prepared in corresponding control rat matrices: control rat plasma, aCSF, control brain, control brain post-vascular supernatant, control brain capillaries. For the preparation of rat plasma and CSF standards, the standard OX26 variants were prepared directly with control matrices. For the preparation of brain tissue standards, the standard OX26 variants were added into the brain homogenate, isolated capillaries, and postvascular supernatant by weight (assuming the matrix's density to be 1) before the incubation with lysis buffer to account for nonspecific binding to the debris. The incubation of the tissue standards and tissue samples were performed at the same time. The isolation and homogenization of brain tissues and capillaries is described in the above section.

The plate was then incubated for 2 h at RT on a plate shaker. After the incubation, the plate was washed and loaded with 30 µL/well of the 1.4 ng/µL of goat anti-human IgG-F(ab')₂ fragment cross-adsorbed F(ab')₂ conjugated with alkaline phosphatase (Cat. # A80-249AP, Bethyl Laboratories, USA) in PBS-Tween buffer. The loaded plate was incubated at RT for 1 h. After the incubation, the plate was washed and loaded with 60 µL/well of *p*-nitrophenyl phosphate solution (1 mg/mL in 1x diethanolamine buffer). The change in absorbance was measured with time (dA/dt) at 405 nm for 45 mins using Filter Max F5 microplate analyzer (Cat. # F5, Molecular Devices, Sunnyvale, CA.). The sensitivity of the ELISA for chimeric mouse-human OX26 variants and trastuzumab is shown in Supplementary Table 1–5.

Data analysis

AUC vs. time curves (AUC_{0→t-last}) for anti-TfR mAbs' PK in plasma, bISF_{ST}, CSF_{LV}, CSF_{CM}, and brain homogenate were calculated using the linear trapezoidal rule. The standard deviations around mean AUC_{0→t-last} values were calculated using the modified Bailer method³⁹ implemented in WinNonlin 7.0 (Phoenix, Pharsight Corporation, Palo Alto, CA). Statistical significance was determined using Student's *t*-test (two-tailed), and the threshold for the significance was set at *P* value less than 0.05.

ABBREVIATIONS

aCSF	artificial cerebrospinal fluid
AUC	the area under the concentration curve
BBB	blood-brain barrier
BCEC	brain capillary endothelial cell
BCSFB	blood-CSF barrier
bISF	brain interstitial fluid
bISF _{ST}	the ISF at the striatum
CM	cisterna magna
CNS	central nervous system
CPEC	choroid plexus epithelial cell
CSF	cerebrospinal fluid
CSF _{CM}	the CSF at the cisterna magna
CSF _{LV}	the CSF at the lateral ventricles
K _D	equilibrium dissociation constant
LV	lateral ventricles
mAb	monoclonal antibody
PD	Pharmacodynamics
PK	Pharmacokinetics
RMT	receptor-mediated transcytosis
ST	Striatum
t _{1/2}	half-life
TfR	transferrin receptor
TMDD	target-mediated drug disposition

ORCID

Hsueh-Yuan Chang  <http://orcid.org/0000-0002-2076-8477>
 Dhaval K. Shah  <http://orcid.org/0000-0002-0723-6206>

References

1. Pardridge WM. Drug and gene delivery to the brain: the vascular route. *Neuron*. 2002;36:555–58.
2. Chang HY, Morrow K, Bonacquisti E, Zhang W, Shah DK. Antibody pharmacokinetics in rat brain determined using microdialysis. *MABs*. 2018;10:843–53.
3. Garg A, Balthasar JP. Investigation of the influence of FcRn on the distribution of IgG to the brain. *Aaps J*. 2009;11:553–57.
4. Pardridge WM. CSF, blood-brain barrier, and brain drug delivery. *Expert Opin Drug Deliv*. 2016;13:963–75.
5. Shah DK, Betts AM. Antibody biodistribution coefficients: inferring tissue concentrations of monoclonal antibodies based on the plasma concentrations in several preclinical species and human. *MABs*. 2013;5:297–305.
6. Yu YJ, Zhang Y, Kenrick M, Hoyte K, Luk W, Lu Y, Atwal J, Elliott JM, Prabhu S, Watts RJ, et al. Boosting brain uptake of a therapeutic antibody by reducing its affinity for a transcytosis target. *Sci Transl Med*. 2011;3:84ra44.
7. Lajoie JM, Shusta EV. Targeting receptor-mediated transport for delivery of biologics across the blood-brain barrier. *Annu Rev Pharmacol Toxicol*. 2015;55:613–31.
8. Smith MW, Gumbleton M. Endocytosis at the blood-brain barrier: from basic understanding to drug delivery strategies. *J Drug Target*. 2006;14:191–214.
9. Abdul Razzak R, Florence GJ, Gunn-Moore FJ. Approaches to CNS drug delivery with a focus on transporter-mediated transcytosis. *Int J Mol Sci*. 2019;20(12):1–43.
10. Pardridge WM. Blood-brain barrier drug delivery of IgG fusion proteins with a transferrin receptor monoclonal antibody. *Expert Opin Drug Deliv*. 2015;12:207–22.
11. Thuenauer R, Muller SK, Romer W. Pathways of protein and lipid receptor-mediated transcytosis in drug delivery. *Expert Opin Drug Deliv*. 2017;14:341–51.
12. Moos T. Immunohistochemical localization of intraneuronal transferrin receptor immunoreactivity in the adult mouse central nervous system. *J Comp Neurol*. 1996;375:675–92.

13. Freskgård PO, Urich E. Antibody therapies in CNS diseases. *Neuropharmacology*. 2017;120:38–55.
14. Johnsen KB, Burkhart A, Thomsen LB, Andresen TL, Moos T. Targeting the transferrin receptor for brain drug delivery. *Prog Neurobiol*. 2019;181:101665.
15. Niewoehner J, Bohrmann B, Collin L, Urich E, Sade H, Maier P, Rueger P, Stracke JO, Lau W, Tissot AC, et al. Increased brain penetration and potency of a therapeutic antibody using a monovalent molecular shuttle. *Neuron*. 2014;81:49–60.
16. Alata W, Paris-Robidas S, Emond V, Bourasset F, Calon F. Brain uptake of a fluorescent vector targeting the transferrin receptor: a novel application of in situ brain perfusion. *Mol Pharm*. 2014;11:243–53.
17. Moos T, Morgan EH. Restricted transport of anti-transferrin receptor antibody (OX26) through the blood-brain barrier in the rat. *J Neurochem*. 2001;79:119–29.
18. Paris-Robidas S, Emond V, Tremblay C, Soulet D, Calon F. In vivo labeling of brain capillary endothelial cells after intravenous injection of monoclonal antibodies targeting the transferrin receptor. *Mol Pharmacol*. 2011;80:32–39.
19. Bien-Ly N, Yu YJ, Bumbaca D, Elstrott J, Boswell CA, Zhang Y, Luk W, Lu Y, Dennis MS, Weimer RM, et al. Transferrin receptor (TfR) trafficking determines brain uptake of TfR antibody affinity variants. *J Exp Med*. 2014;211:233–44.
20. Haqqani AS, Thom G, Burrell M, Delaney CE, Brunette E, Baumann E, Sodja C, Jezierski A, Webster C, Stanimirovic DB. Intracellular sorting and transcytosis of the rat transferrin receptor antibody OX26 across the blood-brain barrier in vitro is dependent on its binding affinity. *J Neurochem*. 2018;146:735–52.
21. Thom G, Burrell M, Haqqani AS, Yogi A, Lessard E, Brunette E, Delaney C, Baumann E, Callaghan D, Rodrigo N, et al. Enhanced delivery of galanin conjugates to the brain through bioengineering of the anti-transferrin receptor antibody OX26. *Mol Pharm*. 2018;15:1420–31.
22. Yadav DB, Maloney JA, Wildsmith KR, Fuji RN, Meilandt WJ, Solanoy H, Lu Y, Peng K, Wilson B, Chan P, et al. Widespread brain distribution and activity following i.c.v. infusion of anti-beta-secretase (BACE1) in nonhuman primates. *Br J Pharmacol*. 2017;174:4173–85.
23. Martin-Garcia E, Mannara F, Gutierrez-Cuesta J, Sabater L, Dalmau J, Maldonado R, Graus F. Intrathecal injection of P/Q type voltage-gated calcium channel antibodies from paraneoplastic cerebellar degeneration cause ataxia in mice. *J Neuroimmunol*. 2013;261:53–59.
24. Jadhav SB, Khaowroongrueng V, Derendorf H. Microdialysis of Large Molecules. *J Pharm Sci*. 2016;105:3233–42.
25. Levy G. Pharmacologic target-mediated drug disposition. *Clin Pharmacol Ther*. 1994;56:248–52.
26. Triguero D, Buciak J, Pardridge WM. Capillary depletion method for quantification of blood-brain barrier transport of circulating peptides and plasma proteins. *J Neurochem*. 1990;54:1882–88.
27. Lange E. Recovery and calibration techniques: toward quantitative microdialysis. In: Müller M, editor. *Microdialysis in drug development*, AAPS advances in the pharmaceutical sciences series. New York, NY, USA: Springer; 2012. p. 13–33.
28. Jadhav SB, Khaowroongrueng V, Fueth M, Otteneder MB, Richter W, Derendorf H. Tissue distribution of a therapeutic monoclonal antibody determined by large pore microdialysis. *J Pharm Sci*. 2017;106:2853–59.
29. Tibbitts J, Canter D, Graff R, Smith A, Khawli LA. Key factors influencing ADME properties of therapeutic proteins: A need for ADME characterization in drug discovery and development. *MAbs*. 2016;8:229–45.
30. Couch JA, Yu YJ, Zhang Y, Tarrant JM, Fuji RN, Meilandt WJ, Solanoy H, Tong RK, Hoyte K, Luk W, et al. Addressing safety liabilities of TfR bispecific antibodies that cross the blood-brain barrier. *Sci Transl Med*. 2013;5:183ra157,181–112.
31. Karaoglu Hanzatian D, Schwartz A, Gizatullin F, Erickson J, Deng K, Villanueva R, Stedman C, Harris C, Ghayur T, Goodearl A. Brain uptake of multivalent and multi-specific DVD-Ig proteins after systemic administration. *MAbs*. 2018;10:765–77.
32. Yu YJ, Atwal JK, Zhang Y, Tong RK, Wildsmith KR, Tan C, Bien-Ly N, Hersom M, Maloney JA, Meilandt WJ, et al. Therapeutic bispecific antibodies cross the blood-brain barrier in nonhuman primates. *Sci Transl Med*. 2014;6:261ra154.
33. Sade H, Baumgartner C, Hugenmatter A, Moessner E, Freskgard PO, Niewoehner J. A human blood-brain barrier transcytosis assay reveals antibody transcytosis influenced by pH-dependent receptor binding. *PLoS One*. 2014;9:e96340.
34. Louveau A, Plog BA, Antila S, Alitalo K, Nedergaard M, Kipnis J. Understanding the functions and relationships of the glymphatic system and meningeal lymphatics. *J Clin Invest*. 2017;127:3210–19.
35. Pizzo ME, Wolak DJ, Kumar NN, Brunette E, Brunnquell CL, Hannocks MJ, Abbott NJ, Meyerand ME, Sorokin L, Stanimirovic DB, et al. Intrathecal antibody distribution in the rat brain: surface diffusion, perivascular transport and osmotic enhancement of delivery. *J Physiol*. 2018;596:445–75.
36. Dickinson TK, Connor JR. Immunohistochemical analysis of transferrin receptor: regional and cellular distribution in the hypotransferrinemic (hpx) mouse brain. *Brain Res*. 1998;801:171–81.
37. Freskgård PO, Niewoehner J, Urich E. Time to open the blood-brain barrier gate for biologics? *Future Neurol*. 2014;9:243–45.
38. Watts RJ, Dennis MS. Bispecific antibodies for delivery into the brain. *Curr Opin Chem Biol*. 2013;17:393–99.
39. Nedelman JR, Gibiansky E, Lau DT. Applying Bailer's method for AUC confidence intervals to sparse sampling. *Pharm Res*. 1995;12:124–28.